International Journal of Paleopathology 52 (2026) 44–57

Contents lists available at ScienceDirect

International Journal of Paleopathology

journal homepage: www.elsevier.com/locate/ijpp

Differential sampling for genetic analyses of *Treponema pallidum* and for radiocarbon dating in archaeological bone

Karen Giffin [a,*], Ariane Weber [b], Justina Kozakaitė [c], Ronny Friedrich [d], Rimantas Jankauskas [c], Denise Kühnert [b,e], Kirsten I. Bos [a,*]

[a] Max Planck Institute for Evolutionary Anthropology, Leipzig, Germany
[b] Max Planck Institute of Geoanthropology, Jena, Germany
[c] Vilnius University, Vilnius, Lithuania
[d] Curt-Engelhorn-Zentrum Archäometrie, Mannheim, Germany
[e] Robert Koch Institut, Wildau, Germany

ARTICLE INFO

Keywords:
DNA preservation
Treponematosis
Molecular dating
Yaws
Infectious disease

ABSTRACT

Objective: Molecular recovery of *T. pallidum* DNA in dry bone poses methodological challenges. Here we evaluate recovery success from a molecularly confirmed co-infection with yaws (*T. pallidum pertenue*) and plague (*Y. pestis*).
Materials: Pulverised bone from three pathological anatomical elements from individual AGU007 excavated from Aguonų street, Vilnius, Lithuania was used for DNA analysis. Three additional anatomical elements from individual AGU007 were used to obtain radiocarbon dates.
Methods: High-throughput sequencing of bulk DNA content followed by computational analysis. DNA sequencing and genomic analysis following molecular enrichment for *T. pallidum*. Radiocarbon dating combined with computational molecular dating.
Results: *T. pallidum* and *Y. pestis* DNA were identified in a cranial fragment from individual AGU007. Radiocarbon dates from this individual combined with another narrowed the temporal range to the latter part of the 15th century at the 2-sigma level.
Conclusions: Detection of *T. pallidum* DNA in multiple skeletal elements from an individual confirmed to have an active yaws infection at time of death gave further insight into preferred sampling locations for molecular detection of treponemal infections. While the highest molecular recovery came from teeth, the parietal bone provided adequate recovery.
Significance: This research indicates that sampling for molecular analysis of *T. pallidum* infections should include (if available) one tooth and one lesion indicative of active infection at the time of death. Accommodating radiocarbon date probability distributions and Bayesian inference has the potential to increase molecular dating precision.
Limitations: *T. pallidum* DNA preservation is not predictable across the skeleton.
Suggestions for Further Research: We encourage ethical and minimalist sampling strategies for further research.

1. Introduction

The temporal and geographic origins of the *Treponema pallidum* subspecies *pallidum* (causative subsp. of syphilis), *pertenue* (causative subsp. of yaws), and *endemicum* (causative subsp. of bejel), along with *T. carateum* (pinta) are subjects of considerable debate in paleopathology. Several theories have been presented, with most centring on the origin of syphilis (Quétel, 1990). Initially it was proposed that all treponematoses were caused by the same organism, and that differences in clinical presentation arose due to context-specific factors such as environment and hygiene (Hudson, 1946; Hudson, 1963). Molecular evidence has since demonstrated distinct phylogenetic groupings of *T. pallidum* subsp. *pallidum*, *T. pallidum* subsp. *pertenue*, and *T. pallidum* subsp. *endemicum*, albeit with high genome-level conservation (Čejková et al., 2012; Strouhal et al., 2017). Due to the timing of the first purported syphilis outbreak in Europe in the late 15th century, a popular

* Correspondence to: Max Planck Institute for Evolutionary Anthropology, Leipzig, Germany.
E-mail addresses: karen_giffin@eva.mpg.de (K. Giffin), kirsten_bos@eva.mpg.de (K.I. Bos).

https://doi.org/10.1016/j.ijpp.2025.11.002
Received 17 September 2024; Received in revised form 24 October 2025; Accepted 9 November 2025
Available online 2 December 2025

hypothesis assumes that syphilis originated in the Americas and was brought to Europe after 1492 (Baker et al., 1988). Substantial skeletal evidence of treponemal infections in the Americas with secure dating have added weight to this theory; however, confident diagnoses of syphilis based on gross pathology in archaeological bone have been challenged (Baker et al., 1988; Powell Cook, 2005), and the patterns of skeletal lesions in pre- and post-colonial periods is possibly indicative of an epidemiological change in treponemal infections after Columbian contact (Powell and Cook, 2005). It has also been suggested that syphilis may have originated in Africa or Eurasia through zoonotic transfer from an as-yet unidentified animal reservoir and moved with human migration or the transatlantic slave trade. Prior to the epidemic that swept Europe, it may have been misdiagnosed as leprosy, though the potential of misdiagnoses has been challenged (Baker et al., 2020; Cockburn, 1961; Hackett, 1963; Hudson, 1964; Livingstone, 1991). Skeletal lesions consistent with pre-contact *T. pallidum* infection have been reported in Europe (Dutour, 1994) and Asia (Mitchell, 2003), but the absence of radiocarbon dates for some individuals, and broad temporal ranges in calibrated radiocarbon dates for others, coupled with marine reservoir effects, continue to fuel debate (Baker et al., 2020; Cole and Waldron, 2011; Cole et al., 2014; Erdal, 2006; Harper et al., 2011; Powell and Cook, 2005; Rao et al., 1996).

Discussions on the origin of treponematoses have largely centred on the diagnostic specificity of skeletal lesions that develop during the course of chronic treponemal infection. Similarities in the skeletal manifestations of yaws, bejel, and syphilis can confound diagnoses (Hackett, 1975; Ortner, 2003), and distinction can be further compromised when skeletal elements that could potentially permit differentiation are absent. Caries sicca, cranial lesions considered strongly suggestive of treponematosis, are present in each of the three subtypes of treponemal infection (Hackett, 1975; Ortner, 2003). Although the most disfiguring lesions are considered attributable to advanced stages of syphilis, less than 20 % of infected individuals are expected to display pathological skeletal lesions (Aufderheide and Rodriguez-Martin, 1998; Steinbock, 1976). While dental defects such as Hutchinson's incisors and Moon's molars are considered pathognomonic for syphilis, their presentation is thought limited to congenital infections, and dental wear may limit their identification in adults (Hillson et al., 1998; Hutchinson, 1858; Moon, 1877). Additionally, commingling of remains, overall skeletal preservation, and taphonomic effects can impact differential diagnoses.

Molecular analyses have the potential to both confirm a past treponemal infection and provide strain-level resolution of the pathogen (Bos et al., 2019). Early molecular recovery efforts for treponemal pathogens had limited successes, generating pessimism in diagnostic potential for this infection (Bouwman and Brown, 2005; Kolman et al., 1999; von Hunnius et al., 2007). In recent years, however, significant advancements in enrichment technologies combined with next-generation sequencing have ultimately permitted the rare molecular confirmation of treponemal disease in archaeological tissues and the reconstruction of ancient treponemal genomes. Thus far, syphilis, bejel and yaws have been molecularly confirmed in both Europe and North America, and studies have revealed a geographic distribution of both bejel and yaws outside of their known present-day contexts (Barquera et al., 2020; Barquera et al., 2024; Giffin et al., 2020; Majander et al., 2020; Majander et al., 2024; Schuenemann et al., 2018). Despite the acknowledged contribution that ancient DNA would provide in addressing unresolved questions surrounding treponemal history (Baker et al., 2020; Joseph and Lindo, 2023), the published literature is limited to only a small number of ancient genomes (Barquera et al., 2020; Barquera et al., 2024; Giffin et al., 2020; Majander et al., 2020; Majander et al., 2024; Schuenemann et al., 2018). While an American origin for the presently defined members of *T. pallidum* has recently been proposed (Barquera et al., 2024), questions persist regarding the distribution of currently extinct forms of infection, as well as the chronology of introduction of yaws, bejel, and syphilis to Europe, and the relative global health impact each had in the past. Moreover, multiple ancient treponemal genomes suffer from poor molecular preservation, which can limit resolution on establishing evolutionary relationships between some strains and further confirms earlier assumptions regarding low molecular recovery of this pathogen (Bouwman and Brown, 2005; Majander et al., 2020; Schuenemann et al., 2018).

Owing to challenges in molecular retrieval of *T. pallidum* in non-viable tissues, resolution of persisting inquiries may require sampling of many individuals. Given the destructive nature of chemically-based bioarchaeological investigations, it is of ethical benefit to investigate optimal sampling location(s) of archaeological human remains for a given application to ultimately reduce the impact upon these irreplaceable resources. Previous studies have explored options for improving endogenous human ancient DNA recovery (Parker et al., 2020; Pinhasi et al., 2015). A parallel approach with pathological specimens is more complex, as stage of infection and bacterial distribution within an individual will impact the success of molecular recovery. Results are also likely to vary based on the pathogen's distribution within the body's tissues, as well as age-at-death and preservation state of the host's remains. Recent studies have considered differential preservation of *Brucella melitensis* (Hider et al., 2022) and *Plasmodium falciparum* (Llanos-Lizcano et al., 2025) across skeletons of infected individuals. Here, we investigate the molecular recovery of ancient treponemal DNA through molecular evaluation of several pathological skeletal elements from an individual known to have had a haemotogenous infection of *T. pallidum* subsp. *pertenue* at their time of death (Giffin et al., 2020). Additionally, we explore the reproducibility of radiocarbon measurements through examination of the differential radiocarbon data from several skeletal elements of this individual. Results are then integrated with available ancient *T. pallidum* subsp. *pertenue* DNA data to gain deeper insights into the recent history of its evolution.

2. Materials and methods

The undocumented burial site (not mapped in 18th-19th-century documents, Fig. 1) was discovered in 2006 and 2007 in Aguonų St. 10, Vilnius, Lithuania. Historically, the site was located outside the city walls and was most likely situated on top of a high sandy hill. However, due to the gradual subsidence of the hill over time, the graves were subsequently discovered at a depth of 0.4–0.6 m below the current ground surface. By the time of the discovery, the site had already sustained extensive damage during the construction of the nearby factory Komunaras (Žukovskis, 2007a). Consequently, the human remains were either partially or severely destroyed. During the archaeological survey, it was determined that the burial site contained multiple mass graves, with up to 15 individuals in a single grave. A total of 119 burials and 216 individuals were exhumed, including 75 males, 62 females, 73 non-adults, and 6 individuals with indeterminate sex (Žukovskis, 2007a, 2007b). Only 23 individuals were buried in coffins, and the remainder were laid to rest in the ground (Žukovskis, 2007a, 2007b). While the majority of bodies were found in an extended position, the arms were positioned in different ways, including folded across the chest, crossed over the pelvic bones, or stretched along the side of the body. However, in five graves the bodies were positioned in an unconventional manner: laying on their side, with limbs arranged in a disorderly fashion (Žukovskis, 2007a). No perimortem injuries that could be associated with mass graves were identified among the individuals. The site was dated to the 15th or 16th century based on a few burial items that were only found during the 2006 excavation. These included a leather purse with metal plates and buttons, three pins, two belt buckles, two rings, fragments of three knives and one pair of scissors, and a penny (denarius) of Grand Duke Alexander of Lithuania (1492–1506) (Žukovskis, 2007a).

Archaeologists hypothesised that the site could be indicative of an outbreak of an epidemic, given the predominance of mass inhumations,

Fig. 1. Vilnius city map by Johann Georg Maximilian Fürstenhof, 1737. "*A*." represents the Neris River. The yellow circle indicates the approximate location of the Aguonų St. 10 site. Scale not included in the original; approximate value added here.

the absence of funerary items, and the absence of perimortem injuries that could be associated with the deaths of the analyzed individuals (Žukovskis, 2007a, 2007b).

In a previous investigation, high amounts of *T. pallidum* subsp. *pertenue* DNA were identified in individual AGU007 excavated from Aguonų street, Vilnius, Lithuania (Table 1) (Giffin et al., 2020;

Table 1
Pathogen DNA preservation variation in captured libraries (either to *T. pallidum* subsp. *pallidum* or *Y. pestis*) from the teeth of Aguonų street individuals (data from Giffin et al., 2020).

Individual	Organism	Tooth processing group	Human Endogenous Content in Unenriched non-UDG Library (%)	Tooth Number (FDI)	Raw Reads Post-capture	Target DNA (%)	Mapped Reads post Duplicate Removal (%)	Mean Fold Genomic Coverage	Percentage of Genome Covered at 3X (%)
AGU007	*Treponema*	A	7.7	48	41012302	4.2	0.31	6.7	92.6
	pallidum	B	70.0	28	45771712	8.6	0.72	21.4	97.7
	Yersinia	A	7.7	48	17223958	5.3	0.91	2.0	31.5
	pestis	B	70.0	28	23998414	40.1	9.77	38.0	94.3
AGU010	*Yersinia*	A	1.2	38	8970962	3.4	0.25	0.3	1.1
	pestis	B	5.3	48	24725162	28.0	5.99	20.8	93.5
AGU020	*Yersinia*	A	0.3	18	14397991	4.9	0.92	1.7	23.7
	pestis	B	0.1	48	19925684	1.3	0.04	0.1	0.1
AGU025	*Yersinia*	A	2.4	38	8165586	6.8	0.76	0.8	6.1
	pestis	B	0.4	28	23621324	27.2	3.60	14.4	93.7

Žukovskis, 2007a, 2007b). Morphological analyses of the skeletal remains were initially performed at Vilnius University. The pathological changes were recorded on the endocranial surface of the skull. Active lesions, identified as new and irregular bone formation, light in colour compared to the rest of the bone, were observed on the inner surface of the frontal bone and on fragments of the parietal bones (Fig. 2C). The lesions were deep and dense, though affecting less than 50 % of the observed bone surface. Healed periosteal reaction and subperiosteal new bone formation with abnormal cortical porosity were observed in the right humerus and ulna. The lesions were localised and involved only the distal portion of the humerus and the proximal portion of the ulna. The pathological changes covered the posterior surface of the humerus; thickening of the subperiosteal active lesion was particularly pronounced at the medial and lateral supracondylar crests (Fig. 2B). Similar changes were noted in the ulna, particularly at the olecranon and ulnar tuberosity (Fig. 2D). There were no pathological changes in the right radius. The indicated pathological changes were visible only on the right side; the left humerus was unaffected. The left ulna and radius were absent and only the upper portion of the skeleton was available for analysis. The lesions observed are consistent with treponematosis, with the cranial lesions being more specifically suggestive of *T. pallidum* infection (Aufderheide and Rodriguez-Martin, 1998; Hackett, 1976; Ortner, 2003).

Sampling and laboratory processing were performed on site at Vilnius University, in the ancient DNA laboratory facilities of the Max Planck Institute for Evolutionary Anthropology in Jena, Germany, and the radiocarbon laboratory at the Curt-Engelhorn-Zentrum Archäometrie in Mannheim, Germany (CEZA). All DNA amplifications were carried out in the modern DNA lab facilities of this institution. Bone powder was collected using a dental drill and bit at low speed from each skeletal element displaying a bone lesion. The first aliquot of bone powder (16.6 mg, AGU007.C) was acquired by drilling the right ulna at the inferior portion of the olecranon process. The second aliquot (34.4 mg, AGU007.D) came from drilling the distal diaphysis of the right humerus. The third aliquot (58.5 mg, AGU007.E) was obtained by drilling the endocranial surface of a parietal bone fragment. A fourth aliquot (87.5 mg, AGU007.H) was comprised of bone powder generated when removing a portion of the parietal bone with a silversmith's saw for radiocarbon dating.

DNA extraction was performed as per Spyrou et al. (2019), modified with the addition of one extraction blank as a reagent blank and an additional processing blank for the bone aliquots extracted (Spyrou et al., 2019).

Double-stranded Illumina libraries were prepared according to established protocols (Meyer and Kircher, 2010) from 10μL of DNA extract and sequenced on an Illumina HiSeq 4000 to an approximate depth of 20 million reads. Sequencing data were mapped in EAGER (Peltzer et al., 2016) against the Nichols reference for *T. pallidum* subsp. *pallidum* (NC_021490.2) and then screened in parallel for the presence of pathogen DNA using the MEGAN Alignment Tool (MALT) and Heuristic Operations for Pathogen Screening (HOPS) pipelines (Table 2, Table 3) (Herbig et al., 2016; Hübler et al., 2019; Peltzer et al., 2016). The MALT database used for query was constructed in 2017 from a custom set of RefSeq genomes that contains bacteria, viruses and eukaryotes (ftp://ftp.ncbi.nlm.nih.gov/genomes/refseq/). HOPS assessed the quality of the taxonomic calls made by MALT. Taxonomic assignments in HOPS were based on a minimum 90 % identity filter and a customised list of pathogens.

Uracil-DNA-Glycosylase (UDG)-treated libraries (Briggs et al., 2009; Rohland et al., 2015) were later prepared from 40 μL of DNA extract for the elements where a treponemal signal was detected by either MALT or HOPS. The UDG-treated libraries and all non-UDG libraries were captured for *T. pallidum* according to previously described methods (Schuenemann et al., 2018). The UDG-treated library for the third left maxillary molar (AGU007.B) generated for the work presented in Giffin et al. 2020 was included in this capture and all subsequent analyses. Captured libraries were sequenced to an approximate depth of 30 million reads on an Illumina HiSeq4000 and mapped to the Nichols

Fig. 2. A) Skeleton of individual AGU007, B) Distal portion of the diaphysis of the right humerus of individual AGU007, C) Endocranial surface of a parietal bone fragment of individual AGU007, D) The olecranon process of the right ulna of individual AGU007. Photographs courtesy of Justina Kozakaitė.

Table 2
Mapping statistics for *T. pallidum*-captured libraries mapped to the Nichols *T. pallidum* subsp. *pallidum* reference. Reads from non-UDG libraries have been clipped by 5-bp from both ends. Mapping parameters were identical for each library type.

Element	Sample ID	Library Type	Raw Reads	Target DNA post Enrichment (%)	Duplicated Mapped Reads (%)	Mapping Reads post Duplicate Removal (reads/M)	Percentage of Genome Covered at 1-fold (%)	Mean Read Length (bp)
Tooth*	AGU007.B	UDG	33,485,320	19.4	89.3	10,914.0	97.9	72.49
Ulna	AGU007.C	Non-UDG	38,246,552	1.3	91.2	28.8	1.2	44.46
Humerus	AGU007.D	Non-UDG	30,442,896	1.6	86.8	38.9	1.1	41.08
Parietal fragment	AGU007.E	Non-UDG	26,226,078	2.3	95.1	71.6	4.3	49.76
		UDG	32,584,662	2.1	90.7	111.6	13.2	49.54
	AGU007.H (sawing powder)	Non-UDG	24,360,334	1.7	89.4	56.4	2.5	51.69
		UDG	36,875,088	0.9	92.1	22.2	2.7	49.74

* new sequencing data from maxillary molar of individual AGU007 generated for this study (Supplementary Information A and Supplementary Information B: Table B.7)

Table 3
Unique DNA reads from the *T. pallidum*-enriched libraries from individual AGU007, assigned in HOPS

Powder	Library Type	Unique Matching DNA Reads in HOPS (reads per million raw sequencing reads)		
		Treponema	*Treponema pallidum* subsp. *pallidum*	*Yersinia pestis*
AGU007.B	UDG	267	259	38
AGU007.C	Non-UDG	34	2	0
AGU007.D	Non-UDG	29	0	0
AGU007.E	Non-UDG	45	29	2
	UDG	80	34	0.4
AGU007.H	Non-UDG	41	11	1
	UDG	33	7	0

reference for *T. pallidum* subsp. *pallidum* in nf-core/eager (Table 2) (Fellows Yates et al., 2021).

In Giffin et al. 2020, the initial 2-sigma calibrated radiocarbon date interval acquired from the right mandibular third molar from individual AGU007 was broad, 1463–1632 cal CE. This ^{14}C date encompasses a time period where the IntCal20 radiocarbon calibration curve is bimodally distributed (Supplementary Information A: Figure A.1), which leads to large intervals in estimated chronological age. Calibrated 2-sigma date ranges from two other individuals from this burial site were substantially narrower, 1435–1477 cal CE for individual AGU010 and 1434–1475 cal CE for individual AGU020 (Giffin et al., 2020), where calibration of ^{14}C data corresponded to an area without multiple peaks in the calibration curve. Terrestrial calibration curves were used for these individuals, as Vilnius is not a coastal site. While the city hosts a freshwater river, isotopic data from its inhabitants representing the 13th to 18th centuries, inclusive of individuals interred in the Aguonų street burial ground, demonstrate a dominance of terrestrial protein dietary sources (Brindzaitė et al., 2025). Aquatic inputs are considered as one possible reason for a slight increase in human δ^{15}N values starting in the 16th century, with historical data supporting consumption of local freshwater species among elites (Brindzaitė et al., 2025). While the archaeologically inferred period of use of the cemetery encompasses the 16th century, the lower socioeconomic status of the population interred in Aguonų is in line with a reduced consumption of imported fish species, alongside a possible modest inclusion of freshwater species in the omnivorous diet. Regardless, aquatic consumption was considered too low to warrant quantitation of a freshwater reservoir effect for the individuals considered here.

Of note, identical *Yersinia pestis* genomes were recovered from both individuals AGU007 and AGU010. As clonal second pandemic *Y. pestis* strains have only been observed within the context of single mortality events (Bos et al., 2011; Spyrou, Bos, et al., 2019; Spyrou, Keller, et al., 2019; Spyrou et al., 2016), the identical genomes suggest these two individuals died within a short time interval, or most parsimoniously during the same outbreak of plague (Giffin et al., 2020; Spyrou, Keller, et al., 2019; Spyrou et al., 2016). In contrast, while individual AGU020 shared a similar 2-sigma radiocarbon date range with individual AGU010, the *Y. pestis* genome isolated from this individual had at least three additional derived SNPs (single nucleotide polymorphisms), suggesting death in a subsequent mortality event (Giffin et al., 2020). The C:N ratio for individual AGU007's tooth collagen was 5.0, thus indicating a potential influence of collagen degradation on dating accuracy (Ambrose, 1990; van Klinken, 1999), and a possible reason for incongruency between the radiocarbon dates of individuals AGU007 and AGU010, given their identical *Y. pestis* genomes. This motivated an investigation into consistency in radiocarbon dates based on multiple skeletal elements from individual AGU007. To achieve this, several elements were analyzed: a rib (AGU007.F), a vertebra (AGU007.G) and a disarticulated portion of the parietal bone (AGU007.I).

Radiocarbon dating was performed on extracted collagen from whole-bone material weighing 500 to about 1500 mg. The collagen extraction followed previously published procedures (Brown et al., 1988). Collagen was thereafter combusted and the resulting CO_2 was reduced to graphite using commercially available graphitisation systems AGE3 (IonPlus). Dating was performed on graphite targets by Accelerator Mass Spectrometry (AMS) (Kromer et al., 2013). Conventional ^{14}C ages were converted into calibrated dates using the calibration dataset IntCal20 (Reimer et al., 2020) and the calibration software Oxcal 4.4.4 (Bronk Ramsey, 2009, 2017). The calibration procedure of the software OxCal employs the probability method where the probability distribution of the analytically derived ^{14}C age is converted into a probability distribution of calendar dates (the so called calibrated ^{14}C dates). Published dating results that did not use the current calibration dataset (Giffin et al., 2020) were re-calibrated. Results are presented in Table 4. Calibrated ^{14}C dates are stated from this point forward as 2-sigma date ranges, reflecting 95.4 % probability.

Molecular dating of the *T. pallidum* subsp. *pertenue* clade was performed using BEAST v2.6.7 utilising the newly acquired radiocarbon dating data and the list of allele variant calls in the *T. pallidum* dataset from Giffin et al. 2020, with the addition of a second ancient *T. pallidum* subsp. *pertenue* genome from individual SJN003 (Barquera et al., 2020; Giffin et al., 2020). Individual SJN003 had been interred in a mass burial associated with the Hospital Real de San José de los Naturales in Mexico City, Mexico, and is archaeologically dated to between 1531 and 1626 CE, and (Barquera et al., 2020). Results were visualised in R v2023.12.0 + 369 using the ape v5.7–1 and ggplot2 packages (Paradis and Schliep, 2019; R Core Team; Villanueva and Chen, 2019).

Table 4
C^{14} Date ranges and radiocarbon analysis data for the analyzed skeletal elements. Teeth, rib, vertebra, parietal fragment and individual AGU007's element combination analyzed using OxCal v 4.4.4 using atmospheric data from Reimer 2020 (Bronk Ramsey, 2009, 2017; Reimer et al., 2020; Reimer et al., 2013).

Element	MPI Sample ID	CEZA Sample ID	CN Ratio	Collagen Concentration	^{14}C age	Sigma-2 (95.4 % probability) calibrated ^{14}C Date		
						Date Range	Probability	Summarised Date Range (min-max)
				(%)	(YBP)	(cal CE)	(%)	(cal CE)
Tooth	AGU010.A*	MAMS 40326	3.1	3.7	426 ± 19	1435–1479	95.4	1435–1479
Tooth	AGU007.A*	MAMS 40889	5.0	0.5	353 ± 18	1471–1527	42.4	1471–1634
						1554–1634	53.1	
Rib	AGU007.F	MAMS 40702	3.2	12.8	378 ± 21	1451–1523	64.7	1451–1625
						1575–1625	30.7	
Vertebra	AGU007.G	MAMS 40703	3.2	11.7	373 ± 21	1453–1524	60.2	1453–1629
						1573–1629	35.3	
Parietal Fragment	AGU007.I	MAMS 40701	3.2	12.5	374 ± 20	1454–1523	61.9	1454–1625
						1575–1625	33.5	
AGU007** Elements Combined	NA	NA	NA	NA	375 ± 12	1456–1514	68.0	1456–1620
						1590–1620	27.4	

* Results for these elements were also presented previously in Giffin et al., 2020 calibrated with IntCal13.
**Combined elements include rib, vertebra and parietal fragment of individual AGU007 only

3. Results

3.1. Differential pathogen DNA preservation variation in teeth

Our initial study that described *T. pallidum* subsp. *pertenue* and *Y. pestis* retrieval in the Aguonų street collection (Giffin et al., 2020) was based on two teeth from each of four individuals (Table 1). These were processed in two sets, group "A" and group "B" teeth. At a sequencing depth of approximately 40 million reads, the *T. pallidum*-enriched library from the third right mandibular molar of individual AGU007 (AGU007.A) yielded a 6-fold mean coverage *T. pallidum* subsp. *pertenue* genome, whereas the enriched library from the third left maxillary molar of the same individual (AGU007.B) yielded a genome with a mean coverage of 21-fold at a comparable sequencing depth (Giffin et al., 2020). The greater genome coverage of AGU007.B was expected since prior to enrichment, this library had 10-fold more human DNA content than its counterpart: 7.7 % vs 70.0 % for AGU007.A and AGU007.B, respectively (Table 1) (Giffin et al., 2020). A similar relationship between pathogen recovery and human DNA content was observed for *Y. pestis* in three of the four individuals who yielded genomic data (Table 1). For AGU025, human DNA preservation in the group "B" tooth was 6-fold lower than its preservation in the group "A" tooth, but pathogen DNA recovery was 4-fold higher (Table 1). Overall, regarding molecular recovery of pathogen DNA, group "B" teeth tended to outperform those from group "A", which could indicate a batch effect in efficiency of DNA extraction or library preparation. This trend, however, was not observed in teeth from individual AGU020, where the group "A" tooth had a higher recovery of both pathogen and host DNA than that from group "B". Taken together, these results indicate stochasticity in ancient DNA recovery for both host and pathogen content between teeth from the same individual.

3.2. Differential pathogen DNA preservation in the ulna, humerus, and cranium of individual AGU007

Approximately 20 million reads from the unenriched libraries from individual AGU007's ulnar lesion (AGU007.C), humeral lesion (AGU007.D), cranial fragment lesion (AGU007.E), and cranial fragment residual sawing powder (AGU007.H) were screened by mapping to the human (hg19), *Y. pestis*, and *T. pallidum* subsp. *pallidum* genomes (Supplementary Information B: Tables B.1-B.6). The sequencing depth was increased by four-fold over that of the original study to increase the likelihood of treponemal DNA detection in taxonomic screening of a library prior to enrichment. This yielded human endogenous DNA ranges of 0.3 – 2.4 %, and detection of reads mapping to both *Y. pestis* (52–233 reads) and *T. pallidum* subsp. *pallidum* (17–29 reads) in all libraries. For comparison to these yields, the endogenous human DNA content in the non-enriched screening library of the tooth (AGU007.B) was previously found to be 70 % (Giffin et al., 2020). Specificity in taxonomic detection of pathogens was more thoroughly evaluated through the MALT/HOPS platform. In this process, few reads were assigned to the node for the genus *Treponema* (Supplementary Information A: Figure A.2). In-depth exploration of read assignments indicated that two libraries, both arising from sampling of the parietal cranial fragment, had weak signals for *T. pallidum*, with four and one fragments detected, respectively (Supplementary Information A: Figure A.2). UDG libraries were subsequently prepared for each of these two DNA extracts and were sequenced to a depth of ca. 12 million reads without enrichment (Supplementary Information B: Table B.5). MALT/HOPS analysis of the UDG libraries revealed fourteen and five fragments, respectively, assigned to *Treponema* at the genus level, with no fragments assigned to the *T. pallidum* subsp. *pallidum* node in either UDG library. Additionally, two fragments were observed in each UDG library at the *Y. pestis* species level (Supplementary Information A: Figure A.2).

To further explore recovery of treponemal DNA, all libraries were then enriched for *T. pallidum* following established methods (Giffin et al., 2020). Raw reads of the non-UDG libraries were trimmed by 5 base pairs at their terminal ends to reduce the influence of DNA damage on mapping (see Supplementary Information A). Sequencing data for *T. pallidum*-enriched libraries from all lesions (AGU007.C, AGU007.D, AGU007.E and AGU007.H), as well as the maxillary molar (AGU007.B, re-sequenced for this study), were then mapped against the Nichols *T. pallidum* subsp. *pallidum* reference (NC_021490.2) in nf-core/eager (Ewels et al., 2020; Fellows Yates et al., 2021) (Table 2, and Supplementary Information A, Supplementary Information B: Table B.7 and Table B.8). Mapping was also performed on untrimmed non-UDG libraries in order to authenticate the results through analysis of DNA read damage patterns (Supplementary Information B: Table B.7, Supplementary Information A: Figure A.3).

Between 818 and 365,458 unique fragments in the *T. pallidum*-enriched libraries mapped to the Nichols reference, yielding genomic coverages of 0.9–97.9 % at 1-fold (Table 2, Supplementary Information B: Table B.7). Of note, only one mapping fragment was observed in the captured negative controls (Supplementary Information B: Table B.9). Nucleotide changes consistent with ancient DNA damage were found in all non-UDG libraries, ranging from 3.3 % to 14.7 % at the first base of the 5' end. While this is considerably lower than the terminal damage seen in the human data, which ranged from 14.5 % to 22.0 % (Supplementary Information B: Tables B.1 and B.7), the influence of

potential non-target reads in the *T. pallidum* capture data should be considered. Despite the low recovery of unique fragments in the cranial sawing powder (AGU007.H), reads from this library covered a larger percentage of the *T. pallidum* subsp. *pallidum* reference genome compared to those from the libraries from the ulnar and humeral lesions (Table 2). This trend may reflect stacking of reads over conserved regions in the datasets from the ulna and humerus, which can occur when non-target molecules from a closely related organism are co-enriched during the capture process. The higher breadth of genome coverage from the cranial powder may also partly result from its greater mean fragment lengths (49.54–51.69 bp) compared to those from AGU007.C and AGU007.D (44.46 bp and 41.08 bp, Table 2).

Taxonomic assignment of captured reads in MALT and HOPS, performed after removal of reads mapping to the human genome (hg19), revealed that the numbers of unique treponemal reads recovered from the ulna and humerus were indeed lower than those recovered from the cranial portions and the maxillary molar (Table 3). This is consistent with the conclusion of off-target reads mapping in the datasets from the ulna and humerus. Taxonomic assignment in MALT and HOPS was performed on DNA reads following removal of reads aligning to hg19. Damage consistent with ancient DNA was observed in reads from all *T. pallidum*-captured non-UDG libraries at both the *Treponema* genus node level (ranging from 17.6 % to 29.4 % at the 5' and 3' ends, Supplementary Table B.10) and the *T. pallidum* subsp. *pallidum* species node (ranging from 19.2 % to 31.6 % at the 5' and 3' ends, Supplementary Information B: Table B.10). Read assignments in the maxillary molar dominated in this analysis, as observed in the mapping (Tables 2 and 3). No *T. pallidum* subsp. *pallidum* reads were recovered in the dataset from the humerus (AGU007.D), suggesting that reads identified in the mapping derived from a non-target source.

Reads assigned to *Yersinia pestis* were also detected in our HOPS analysis of the *T. pallidum*-captured libraries from the maxillary molar (AGU007.B) and the parietal fragment (AGU007.E) (Table 3). Predictably, the highest number of DNA reads assigned to *Y. pestis* were observed in the tooth. Consistent with its higher recovery of *T. pallidum* subsp. *pallidum* DNA compared to the ulna or humerus, the parietal fragment (AGU007.E) also yielded *Y. pestis* reads, detected in both its non-UDG and UDG libraries. One *Y. pestis* fragment was also detected in the non-UDG *T. pallidum*-enriched library of the cranial sawing powder (AGU007.H) (Table 3).

The UDG library generated from the parietal fragment sawing powder (AGU007.H) had a lower proportion of reads assigned to *T. pallidum* subsp. *pallidum* in comparison to the analogous non-UDG library, consistent with the lower endogenous treponemal DNA that was detected in the UDG library via mapping (Table 2, Supplementary Information A: Figure A.2, Supplementary Information B: Table B.5). Increased sequencing depth would likely not increase genome coverage in any of the skeletal elements as duplication rates are high, 86.8–95.1 %.

3.3. Phylogenetic analyses

Data generated in this study were analyzed alongside the set of modern of *T. pallidum* genomes considered in Giffin et al. 2020 (n = 29) with inclusion of the additional ancient *T. pallidum* subsp. *pertenue* genome from individual SJN003 from colonial Mexico reported in Barquera et al., 2020[28] (Supplementary Information B: Table B.11). Variant positions were called against the Nichols *T. pallidum* subsp. *pallidum* reference at a minimum coverage of 5-fold and genotyping quality of 30 in MultiVCFAnalyzer v0.85 (https://github.com/alexherbig/MultiVCFAnalyzer). Allele variants called through application of this filter were used in the construction of a phylogenetic tree (Supplementary Information B: Table B.12). Ancient *T. pallidum* subsp. *pertenue* genomes CHS119 (Turku) from Majander et al. 2020 and 133 from Schuenemann et al. 2018 were excluded from this analysis due to their low coverage (Supplementary Information B: Table B.12), which can lead to erroneous calling of single nucleotide polymorphisms from non-target mapping reads, aDNA damage, or polymerase/sequencing errors during molecular processing. In higher coverage genomes, greater numbers of fragments align to a given position, thus diluting such erroneous signals when the heterozygosity tolerance in MultiVCFAnalyzer is adjusted to be low.

T. pallidum genomes are known to recombine, which introduces challenges in resolving phylogenetic relationships (Arora et al., 2016; Pětrošová et al., 2012; Schuenemann et al., 2018). Recombinant positions identified in Giffin et al. 2020 were excluded (Giffin et al., 2020). A complete deletion maximum likelihood tree was constructed in RAxML-NG v 0.9.0 using a GTR+GAMMA substitution model and 1000 bootstrap replicates (Fig. 3) (Kozlov et al., 2019).

The two ancient genomes of individuals AGU007 and SJN003 cluster together and share a common ancestor with the modern Ghanian and CDC genomes, to the exclusion of other *T. pallidum* subsp. *pertenue*. Previously, five SNP positions that separated individual AGU007 from the most recent common ancestor of yaws were identified following investigation of the variant positions present in the yaws genomes included in the phylogenetic analysis (Giffin et al., 2020). Two of these positions were unique to individual AGU007's genome (Giffin et al., 2020). The other 3, namely positions 6654, 246339 and 878279 define the yaws clade in both the current and previous analysis. Genomes from individuals SJN003 and AGU007 share the alternative allele state with the Ghana and CDC modern genomes at each of these positions (Supplementary Information A: Fig. 2A, Supplementary Information B: Table B.13), and the genome from individual SJN003 has additional unique SNPs that have accumulated since its divergence from a common ancestor with the genome from individual AGU007.

Phylogenetic analysis of the data from parietal fragments AGU007.E and AGU007.H was made possible by pooling the trimmed reads from their non-UDG libraries with their UDG libraries and then computationally increasing the data to three fold coverage to permit SNP calling in MultiVCFAnalyzer v0.85 (https://github.com/alexherbig/MultiVCFAnalyzer) (Supplementary Information A). Despite the low genome coverage of approximately 20 % when pooled together (Table 1), thirteen positions were identified that supported its placement within *T. pallidum* subsp. *pertenue* (yaws) (Supplementary Information A: Figure A.4, Supplementary Information B: Table B.14).

3.4. Differential radiocarbon age determinations from a tooth, rib, vertebra, and parietal fragment of individual AGU007

This study considered new radiocarbon ages and dates obtained from the ulna, humerus, and cranial fragment alongside new ages and IntCal20-calibrated dates for one tooth from each of two individuals initially calibrated with IntCal13 in Giffin et al., 2020 (Reimer et al., 2020; Reimer et al., 2013) (Supplementary Information A: Figure A.1, Table 4). The radiocarbon results of all queried skeletal elements for individual AGU007 were highly similar, despite variation in collagen preservation between the tooth and the other elements. The tooth root had only 0.5 % collagen whereas the other elements varied between 11.7 % and 12.8 % (Table 4). The ratio of carbon to nitrogen (C:N ratio) in the published radiocarbon analysis of the tooth (Giffin et al., 2020) was also elevated at 5.0, further demonstrating some degradation of the collagen, and a possible influence of diagenesis, which can affect the accuracy of the radiocarbon date (Ambrose, 1990; van Klinken, 1999) (Table 4). In contrast, the C:N ratios of the bone elements were all 3.2, within the ideal range of 2.6–3.3 (Ambrose, 1990; van Klinken, 1999).

Taking advantage of the availability of multiple ^{14}C ages from one individual, the ages can be analyzed together (error-weighted mean) in IntCal20, OxCal v 4.4.4 (Bronk Ramsey, 2009, 2017) resulting in a combined ^{14}C age with a reduced uncertainty. ^{14}C ages of individual AGU007, inclusive of that from the tooth, were all consistent within their uncertainties, passing a chi-square (χ^2) test with test statistic T = 1.1 and 3 ° of freedom. The chi-square test is automatically provided

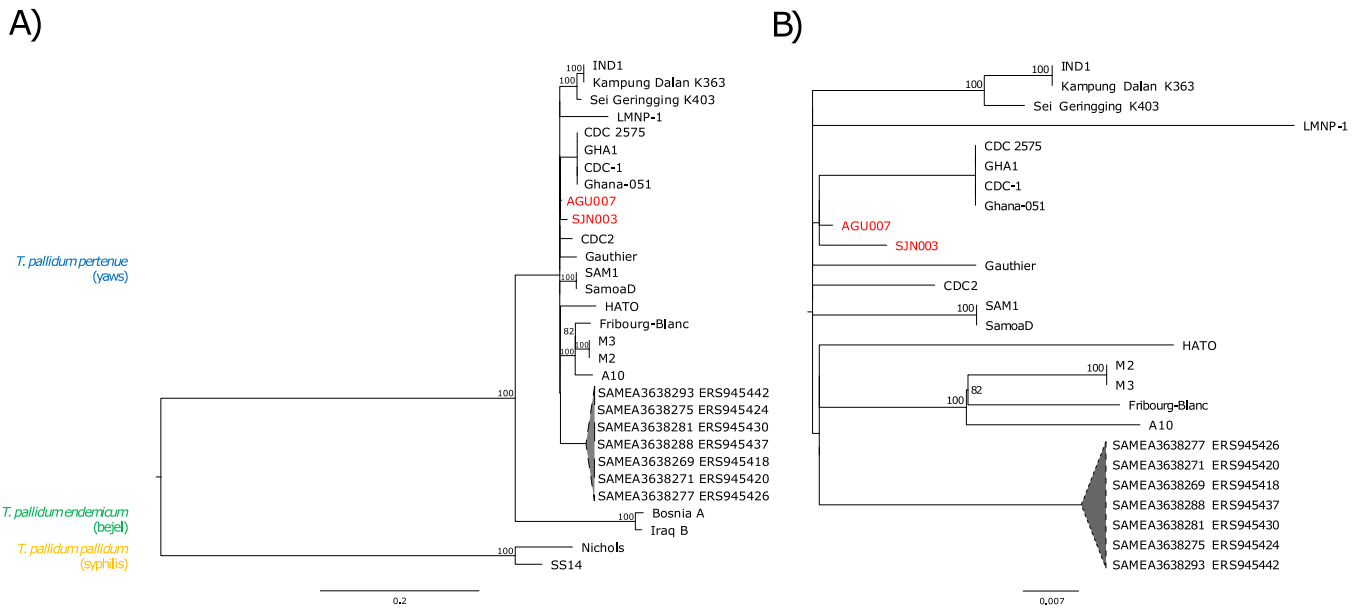

Fig. 3. A) Complete deletion maximum likelihood phylogenetic tree of the *T. pallidum* subsp. *pertenue* clade constructed using 1000 bootstrap replicates, rooted with *T. pallidum* subsp. *pallidum*. B) Enlarged view of the *T. pallidum* subsp. *pertenue* clade. Ancient genomes names are shown in red, modern genome names are shown in black. Bifurcated nodes with statistical support of more than 80 % are indicated. The scale represents mean DNA nucleotide substitutions per site in the single nucleotide polymorphism (SNP) alignment given a general time-reversible plus gamma distribution (GTR+GAMMA) DNA nucleotide substitution model.

by OxCal's "R_Combine" function (Shennan, 1988). Using the ^{14}C ages of individual AGU007's skeletal elements, excluding the tooth due to its elevated C:N ratio, yielded a combined ^{14}C age of 375 ± 12 YBP (see Supplementary Information A), and a calibrated date range spanning 1456–1620 cal CE (2-sigma) (Table 4). This relatively wide range is again caused by the bimodal peaks, or wiggle, characteristic of this period in the IntCal13 and IntCal20 calibration curves. This differed from the IntCal13 2-sigma date range previously reported for this individual, which was 1463–1632 cal CE for AGU007.A alone, and 1447–1616 cal CE when calibrated together with individual AGU010 (Giffin et al., 2020).

To accommodate the finding of identical *Y. pestis* genomes in individuals AGU007 and AGU010 (Giffin et al., 2020), a phenomenon thus far only observed in contemporaneous single mortality events (Spyrou, Keller, et al., 2019), a Bayesian approach performed within OxCal 4.4 was used to better constrain the radiocarbon dates (Supplementary Information A). The prior of the Bayesian model prescribes how the radiocarbon data of the two individuals AGU007 and AGU010 relate to each other. Here, we assume that the radiocarbon dates are in no specific order and are therefore grouped within a phase where the death of the individuals happened within a time period of 25 ± 25 years to account for varying mutation rates of *Y. pestis,* as has been observed within the phylogeny of the second pandemic branch of *Y. pestis* (Spyrou, Keller, et al., 2019). This analysis yields a modelled interval of 1453 – 1497 CE for the death of individual AGU007 (Table A.1, Fig. 4).

3.5. Molecular dating

The refined radiocarbon intervals obtained by the combination of individual AGU007's skeletal elements and by the Bayesian model were then used in a revised molecular dating approach to better estimate the emergence date of the yaws clade. We note that a recent publication has suggested a common American origin for the three known *T. pallidum* sublineages (Barquera et al., 2024). While this would imply a post-1493

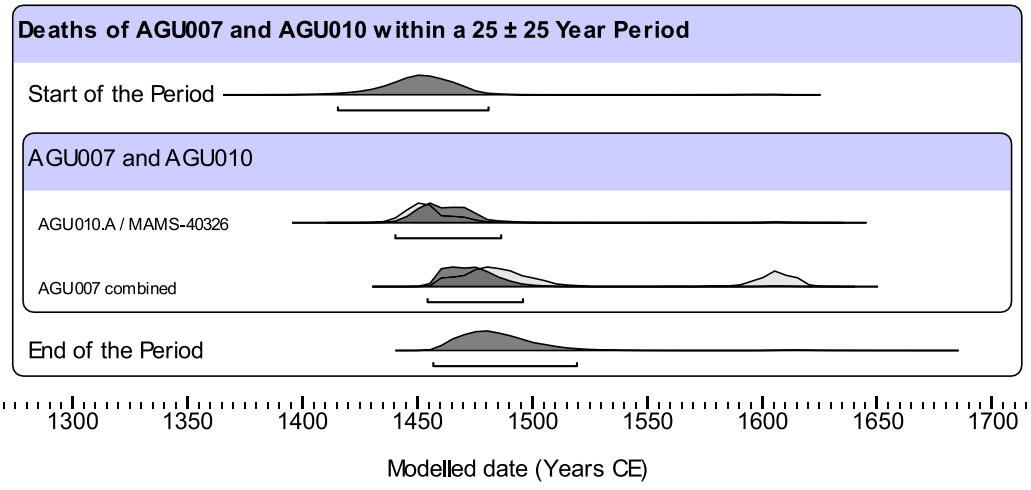

Fig. 4. Bayesian modelling of the death interval for both individuals AGU007 and AGU010 in OxCal 4.4.4 calibrated using IntCal20. Distributions in dark grey represent the modelled intervals and light grey distributions represent the input radiocarbon date ranges at 95 % confidence.

date for individual AGU007's genome, we have utilised the 2-sigma bound date interval in these analyses for more transparent comparison with other published dating estimates. The complete deletion alignment with SNPs called at 5X generated for phylogenetic inference in Giffin et al. 2020 was used here, both with and without the inclusion of the genome from individual SJN003 archaeologically dated to Mexico City's colonial period (1531–1626) (Barquera et al., 2020; Giffin et al., 2020). Ancient genomes from individuals 133 and CHS119 were excluded on account of their low coverage (Supplementary Information B: Table B.11).

The previous dating analysis of this dataset (Giffin et al., 2020) was based on uniform distributions of the 2-sigma radiocarbon date ranges. Here the BEAST (v2.6.7) configuration file was modified directly to use a less-restrictive normal distribution and include the weighted probabilities within the 2-sigma date ranges (weighted normal) obtained from the combined radiocarbon calibration of individual AGU007 (Table 4). Additionally, BEAST configuration files were generated using a normal distribution and the posterior date for individual AGU007 of 1453–1497 CE obtained via the Bayesian model in OxCal 4.4.4 that constrained the date of death of individuals AGU007 and AGU010 to a 50-year period (25 ± 25 years) (Supplementary Information A: Table A.1). Model averaging and model selection techniques were applied to further inform the choice of the substitution and clock model (Supplementary Information A). These supported the uncorrelated exponentially distributed clock as the best-fitting model, however strong temporal signal was only observed with a strict clock model (Supplementary Figure A.5). Relaxed clock models, however, are often employed as evolutionary rates can vary with time, population size and evolutionary pressures (Douglas et al., 2021; Gillespie, 1994; Loh et al., 2010; Woolfit, 2009). Comparisons were, therefore, made between the exponentially-distributed relaxed clock ("UCED") and strict clock ("strict") models on the outcomes of the time to the yaws most recent common ancestor (TMRCA), the computationally interpolated date range of individual AGU007 yielded in these simulations ("tip dating"), and the mean clock rate (Fig. 5). Comparisons were also made between the date ranges of individual AGU007 used in this study found via Bayesian modelling ("Bayesian") and the weighted probability distribution of individual AGU007 following R-combine ("AGU007 combined") (Fig. 5).

The mean values remained largely unchanged regardless of which clock model was used, but standard deviations in the relaxed clock models (Table 5 and Supplementary Information A: A.2) were generally much broader, which is likely due to the limited information content regarding absolute sampling times in the data in combination with the less-constrained model as observed in this organism in a previous study (Majander et al., 2020). The mean time to the most recent common ancestor (TMRCA) increased slightly in temporal depth from 696 (424–1043, 95 % HPD) YBP under a relaxed clock to 698 (451–1004, 95 % HPD) YBP under a strict clock model that considered the weighted probability distribution obtained through the R-combined date range of individual AGU007 ("AGU007_combined") (Table 5). The interpolated date of the genome of individual AGU007 was the most strongly affected outcome when comparisons were made between using the OxCal Bayesian-model-informed distribution ("Bayesian") and the weighted distribution of the R-combined date ranges of individual AGU007 ("AGU007_combined") (Fig. 5), as expected under its more restrictive prior distribution.

For more thorough evaluation of the effects on temporal signal, the alignment from Giffin et al. 2020 with either the weighted R-Combine age estimate for individual AGU007 or the OxCal Bayesian modelled date range for individual AGU007 were tested using a strict clock both with and without the inclusion of the ancient genome from individual SJN003 (Table 5). With use of individual AGU007's date range from R_Combine, inclusion of individual SJN003's genome in the alignment increased the TMRCA from 698 (451 – 1004, 95 % HPD) to 812 (569–1082, 95 % HPD) YBP (Table 5). In contrast, the yaws TMRCA remained relatively stable by the inclusion of individual SJN003 when the OxCal Bayesian-estimated posterior date for individual AGU007 was considered: yaws TMRCA dates of 837 (611–1097, 95 % HPD) YBP and 838 (603–1106, 95 % HPD) YBP were obtained via exclusion and inclusion of individual SJN003, respectively. Bayesian-estimated date ranges for the death of individual AGU007 in BEAST2 differed only marginally between that obtained via use of the uniform age interval reported in Giffin et al., 2020 and that determined by the weighted normal distribution used in this study, regardless of the inclusion of individual SJN003 (Table 5). The date ranges for the death of individual AGU007 were more constrained with the employment of the OxCal Bayesian-modelled posterior date of individual AGU007, although the inclusion of individual SJN003 had little effect: without individual SJN003 in the alignment, the date of death for individual AGU007 was estimated to be 1455 – 1498 CE with 95 % probability (Table 5), whereas inclusion of individual SJN003 in the alignment yielded a date range of 1453 – 1496 CE at the 95 % highest posterior density level (Table 5). Analogous results under a relaxed clock model for all date ranges considered are given in Supplementary Information A, Table A.2.

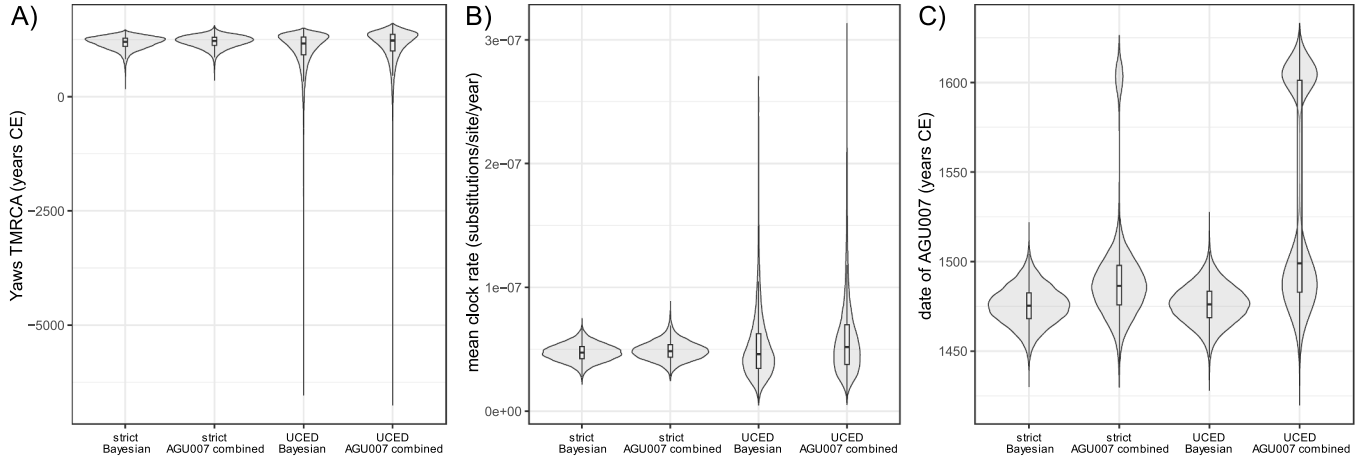

Fig. 5. Clock model and date distribution type effects on A) yaws TMRCA B) mean clock rate, and C) inferred date range of individual AGU007; strict = strict clock, UCED = uncorrelated relaxed clock (exponentially distributed), Bayesian = Bayesian model-informed date distribution, AGU007 combined = weighted mixture distribution of individual AGU007's skeletal elements' R-combined radiocarbon data.

Table 5
Effects of phylogenetic alignment, molecular clock model and prior distribution type on individual AGU007's tip date and TMRCA of yaws.

Sample(s)	Skeletal Element(s)	Radiocarbon Age Combination Method	SNP Alignment Used in BEAST	Radiocarbon Date and Informed Prior Distribution Type	Molecular Clock Model	Bayesian Posterior Tip Date Range for AGU007 (95 % confidence level)	Mean Clock Rate (95 % HPD; substitutions per site per year)	Yaws TMRCA	
								Years Before Present (95 % HPD)	Date (Years CE) (95 % HPD)
AGU007.A*	tooth	NA	Giffin et al. 2020	uniform [U(1456–1616)]	Relaxed	1464–1633 CE	5.8E−8 (2.7E−8, 8.8E−8)	696 (424, 1043)	1324 (977–1596)
AGU007.F, AGU007.G, AGU007.I	rib, vertebra, parietal fragment	AGU_combined	Giffin et al. 2020	weighted normal [0.71*N(1485, 15) + 0.29*N(1605, 7.5)]	Strict	1466–1620 CE	5.8E−8 (3.6E−8, 8.2E−8)	698 (451, 1004)	1317 (1011–1564)
			Giffin et al. 2020 + SJN003	weighted normal [0.71*N(1485, 15) + 0.29*N(1605, 7.5)]	Strict	1455–1604 CE	4.9E−8 (3.4E−8, 6.4E−8)	812 (569, 1082)	1203 (933 – 1446)
AGU007.F, AGU007.G, AGU007.I, AGU010.A	rib, vertebra, parietal fragment, tooth	Bayesian	Giffin et al. 2020	normal 1453–1497	Strict	1455–1498 CE	4.7E−8 (3.4E−8, 6.1E−8)	837 (611, 1097)	1178 (918–1404)
			Giffin et al. 2020 + SJN003	normal 1453–1497	Strict	1453–1496 CE	4.7E−8 (3.4E−8, 6.1E−8)	838 (603, 1106)	1177 (909–1412)

* all data analyzed in 2020

4. Discussion

When sampling skeletal material for pathogenic DNA, pathophysiology of the suspected infectious disease is best considered. Skeletal lesion development during treponemal infection varies according to the individual's physiology, age, stage of disease, and possibly subspecies of the causative pathogen (Aufderheide and Rodriguez-Martin, 1998; DeWitte and Stojanowski, 2015; Ortner, 2003). Initial stages of *T. pallidum* infection involve a local ulceration of soft tissue from where the bacteria enter the bloodstream and become systemic in the secondary phases of yaws, bejel, and syphilis. Many individuals enter a latent phase following systemic spread. If the infection remains untreated, rare cases will proceed to the tertiary phase which can result in significant skeletal involvement and soft tissue damage. However, during the latent and tertiary phases, the bacteria are more rarely detectable in blood, as the organism is sequestered in other tissues (Wang et al., 2018; Wang et al., 2021; Wang et al., 2022).

Morphological detection of treponemal infection in archaeological remains carries challenges, as few skeletal changes are considered pathognomonic. Caries sicca, Moon's molars and Hutchinson's incisors are currently considered to be the most diagnostic lesions (Hackett, 1976; Hillson et al., 1998); however, the rarity of caries sicca development and the restriction of dental pathology to congenital infections limits visibility of treponemal infections in archaeological collections. While long bones are also often affected, the resulting lesions are considered less specific to treponematosis as they can result from other causes of inflammation or circulatory disturbances (Hackett, 1976). As targeted sampling has thus far been required for DNA recovery, these phenomena have left the treponematoses understudied in a molecular context, despite fervent interest in disentangling their evolutionary history.

Though demonstration of *T. pallidum* recovery from archaeological remains is limited to only a handful of publications, successes have been reported from both teeth and skeletal elements, most of which display lesions (Barquera et al., 2020; Barquera et al., 2024; Giffin et al., 2020; Majander et al., 2020; Majander et al., 2024; Schuenemann et al., 2018). Encouragingly, identification is thus possible during both secondary and tertiary stages of infection. Fifteen ancient treponemal genomes have thus far been recovered: while four have come from teeth (Barquera et al., 2020; Barquera et al., 2024; Giffin et al., 2020; Majander et al., 2020), the remaining eleven derive from either the pelvis (n = 1) (Barquera et al., 2024), cranium (n = 2) (Barquera et al., 2024; Majander et al., 2020), or a long bone (n = 8) (Barquera et al., 2024; Majander et al., 2020; Majander et al., 2024; Schuenemann et al., 2018). The highest-covered ancient *T. pallidum* (syphilis) genome thus far was recovered from the *pars petrosa* of a perinatal infant (Majander et al., 2020). Two high coverage genomes from Mexico and Lithuania were recovered from adult teeth (Barquera et al., 2020; Giffin et al., 2020). While all three subclades have now been recovered from archaeological tissues, the number of confirmed yaws cases is worthy of note; four of the fifteen ancient genomes are classified as *T. pallidum* subsp. *pertenue* (Barquera et al., 2020; Giffin et al., 2020; Majander et al., 2020; Schuenemann et al., 2018), and two ancient genomes appear to be descendants of a common ancestor of both bejel and yaws (Barquera et al., 2024). Despite its current status as a rare neglected tropical disease, its past distribution, and possibly its global health impact, differed in the years following its emergence.

Here we explored the recoverability of *T. pallidum* DNA in multiple elements from an individual molecularly confirmed to be infected with *T. pallidum* subsp. *pertenue*, the subspecies currently associated with yaws. Skeletal involvement suggests the individual may have been in the early stages of the tertiary phase, as humeral and ulnar lesions occur during this period, but these can also result from secondary infections from cutaneous ulceration (Ortner, 2003). We attempted to approach our current study as would be done in a naïve sampling in molecular paleopathology, where drilling was performed on three locations with

active lesions to yield ca. 50 mg of bone powder each. Where sawing was necessary, residual sawing powder was collected and processed. Data were analyzed following standard procedures, though with deeper sequencing of the initial bulk DNA screening library (20 million reads as opposed to a more common 5 million reads). This deeper sequencing proved necessary for detection of the *T. pallidum* DNA in the non-enriched screening datasets: as we recovered a maximum of 4 reads in 20 million, down sampling our data to 5 million reads would reduce the average number of reads taxonomically assigned to *T. pallidum* subsp. *pallidum* to a single molecule. Despite this low recovery, enrichment followed by sequencing to standard depths (20 million reads) succeeded in recovering sufficient *T. pallidum* DNA for both authentication through damage patterns and phylogenetic assignment to the *T. pallidum* subsp. *pertenue* (yaws) subclade level. The potential thus exists for molecularly recoverable *T. pallidum* DNA to have been missed in standard pathogen screening of ancient DNA datasets.

The greater retrieval of *T. pallidum* DNA from the parietal fragment, as compared to the ulna or humerus, may allude to the cranium being a focal point for treponemal organisms in later disease stages, in accord with the development of caries sicca. However, changes to the inner table of the cranium, such as the lesions identified in individual AGU007, are more rarely observed (Hackett, 1975). Importantly, our recovery of treponemal DNA in the small mass of powder produced when sawing the parietal fragment (AGU007.H) could suggest molecular recovery from diploë, in addition to inner table cortical bone (AGU007.E). While fragments mapping to *T. pallidum* were identified in the periosteal lesions on the ulna and humerus following enrichment, the number of assigned fragments were substantially reduced with more robust taxonomic assignment of the data, and the breadth of *T. pallidum* genome coverage was substantially lower compared to yields from the tooth or the parietal fragment (Table 2). While overall recovery of both human and pathogen DNA from the maxillary molar was exceptional, human DNA preservation was not a reliable proxy for pathogen recovery in the elements with pathological lesions considered here. While the ulnar lesion had the highest human DNA content of the four screening libraries at 2.4 %, highest treponemal recovery was observed in the parietal fragment and its sawing powder (1.5 % and 0.33 % human DNA content, respectively), suggesting that progression of the infection across the skeleton may play a role in molecular recovery of the bacterium.

We also report on substantial differences in DNA recovery from teeth of the same individual, as evident in the disparity in treponemal genomic coverage of the left maxillary third molar (AGU007.B) and the right mandibular third molar (AGU007.A) (Giffin et al., 2020). The recovery of endogenous human DNA between the maxillary and mandibular third molars of individual AGU007 also differed by an order of magnitude (7.7 % vs 70 %, respectively) (Giffin et al., 2020). It is important to highlight, however, that haematogenous dissemination of *T. pallidum* occurs for a rather brief period in the course of infection, hence teeth may not consistently be a superior source for detection of this pathogen. Recovery of *T. pallidum* DNA from the teeth of individual AGU007 may have been influenced by the *Y. pestis* Gram negative sepsis, which may have reduced the body's defenses to a point where the pathogen entered the bloodstream. Aside from teeth, the parietal fragment was the only other skeletal element to indicate the presence of *T. pallidum* during the screening phase, and subsequent enrichment for *T. pallidum* provided sufficient recovery to confirm the infection.

From the results of previous studies, the analyses presented here, and what is known about the disease progression of yaws, bejel and syphilis, we recommend an ancient DNA sampling strategy for adult individuals that involves at least one tooth accompanied by a skeletal element with a lesion considered consistent with a treponemal infection. Additionally, based on the pathophysiology of *T. pallidum*, lesion sampling should ideally penetrate the medullary cavity of the skeletal element. Due to the treponemes' dissemination via the circulatory system during the secondary phase of the disease, some skeletal lesions develop on the medullary surface and progress to the outer surface of the bone, while others begin in the periosteum (Ortner, 2003). While differential preservation between teeth and low frequency of osseous changes firmly attributable to treponemal infection may provide challenges to following this recommendation, the evidence presented here suggests that this approach is more likely to yield successful analyses. Based on published studies, non-adult remains are highly represented in successful recoveries of treponemal DNA. Six of the ten ancient genomes are from subadult individuals, three are from adults, and one is from an element that lacked features allowing for accurate age-at-death estimation (Majander et al., 2024). Regardless of age at death or skeletal element, there is clear benefit of increased sequencing depth in the screening phase to maximise computational detection of this elusive pathogen.

The finding of *Yersinia pestis* DNA in both the shotgun pathogen screening libraries and captured libraries of the parietal fragment (AGU007.E) suggests that skeletal elements other than teeth may also be suitable for detection of plague infections (Supplementary Figure A.2). While *Yersinia pestis* DNA has been detected in skeletal elements other than teeth (Parker et al., 2023), a broader skeletal survey for this organism has yet to be performed. While this is beyond the scope of the current study, the teeth from individual AGU007 conclusively indicate an active plague infection, and mapping of the shotgun screening libraries to the CO92 *Yersinia pestis* reference genome suggests the ulna, humerus and parietal fragment all have mapping fragments above background levels (Supplementary Table B.3) (Giffin et al., 2020). Given the systemic nature of the sepsis that results from untreated *Yersinia pestis* infection, it is possible that other skeletal elements could serve as sources for *Yersinia pestis* detection, and possibly genome recovery, when teeth are not available.

No significant variations in radiocarbon dates were observed when multiple elements from one individual were analyzed. The four radiocarbon measurements from individual AGU007 are statistically consistent with one another at the 5 % level ($T' = 1.1$, $T'(5\ \%) = 7.8$, $v = 8$) (Ward and Wilson, 1978). Using the rib, vertebra and parietal fragment of individual AGU007, the combined calibrated date of their ^{14}C ages is 1456–1620 cal CE (Table 4). The previously reported date for individual AGU007 in Giffin et al. 2020, 1463–1632 cal CE, which was based on a tooth, was slightly shifted to a more recent time interval compared to dates obtained from the other elements (Table 4). This is likely a result of preservation differences, demonstrated by the tooth's low collagen concentration and high carbon to nitrogen ratio, as these are known to impact radiocarbon dates (Ambrose, 1990; Brock et al., 2010; Hedges and Law, 1989; van Klinken, 1999). All 2-sigma radiocarbon data from this individual support a date of death between the 15th and 17th centuries CE, which limits its refinement to a pre- or post-1493 treponemal infection. However, informing the date of death of individual AGU007 through Bayesian modelling with radiocarbon data from individual AGU010 constrains and reduces this range to the latter part of the 15th century at the 2-sigma level.

The inclusion of the radiocarbon date probability distribution in the molecular dating analysis resulted in only a marginal shift of the yaws TMRCA from 1324 CE (977 – 1596, 95 % HPD) (Giffin et al., 2020) to 1317 CE (1011–1564, 95 % HPD), and had a negligible effect on the BEAST2-estimated age of skeleton AGU007 (Table 5). The inclusion of individual SJN003's data along with the weighted probability distribution for individual AGU007 had a greater effect on this TMRCA, since the mean time of yaws emergence shifted into the early 13th century (1203 CE, 933–1446, 95 % HPD). The same effect, but less pronounced, was observed with the relaxed clock model (Supplementary Information A, Table A.2). The BEAST2-modelled date of death of individual AGU007 was most strongly affected by use of a Bayesian-informed posterior date determined in OxCal that accommodated radiocarbon data from both individuals AGU007 and AGU010, as both are assumed to have died in the same plague outbreak. This constrained the BEAST2-estimated range for individual AGU007's death to the second

half of the 15th century. Importantly, this range was largely unchanged with inclusion of individual SJN003 in the dating analysis, a colonial-era yaws genome from Mexico (Table 5). Similarly, BEAST2 estimates for the yaws TMRCA based on the OxCal Bayesian-modelled date range for individual AGU007 yielded mean values in the late 12th century, a result consistently obtained with either inclusion or exclusion of the genome from individual SJN003. Close agreement in these dates compared to those obtained based on the unmodelled weighted radiocarbon combined date when individual SJN003's data is included shows encouraging congruence between different molecular dating approaches (Table 5).

Estimated ranges for the date of death support a hypothesis that individual AGU007 fell victim to the prolific treponemal outbreak historically reported in late 15th and early 16th century Europe (Quétel, 1990). Archaeological support is given by the age of a coin associated with the burial ground that indicates its use included a period after 1492 (Žukovskis, 2007a). This is consistent with the recent suggestion that *T. pallidum* was introduced to the continent post-1492 (Barquera et al., 2024). The estimated yaws TMRCA further suggests that the known representatives of this sublineage have all descended from a common ancestor that was circulating in the Americas shortly before Columbian contact.

5. Conclusions

Detection of *T. pallidum* DNA in multiple skeletal elements from an individual confirmed to have an active yaws infection at the time of death gave further insight on preferred sampling locations for molecular detection of treponemal infections in archaeological tissues. While highest molecular recovery came from teeth in this case, the parietal fragment, a skeletal element which is known to be a site of lesions highly suggestive of treponemal infection, also yielded positive results. While teeth remain good candidates for isolating ancient treponemal DNA in adults, skeletal elements displaying lesions known to be directly attributable to treponemal infections are also highly viable candidates for successful retrieval of this elusive pathogen. Multiple dating simulations consistently yielded a relatively recent emergence of the yaws subclade, within the last millennium. This study demonstrates the possible benefits of including weighted probability distributions where radiocarbon date ranges are broad due to plateaus or curve reversal (Reimer et al., 2020) in the radiocarbon calibration, particularly if there is a greater proportion of the distribution in a specific portion of the date range. This research also highlights the benefits of refining radiocarbon dates with Bayesian modelling when an individual's date of death can be constrained by another individual from a highly similar or identical context, including simultaneous-deposition multiple burials, close familial relationship, or when individuals share identical genomes for rapidly evolving pathogens. These methods may serve to improve the precision of molecular dating where broad radiocarbon dates are present, and could be tested on rare individuals where date of death is known.

CRediT authorship contribution statement

Giffin Karen L.: Writing – review & editing, Writing – original draft, Methodology, Investigation, Funding acquisition, Formal analysis, Data curation. **Justina Kozakaitė:** Writing – review & editing, Resources, Investigation, Formal analysis. **Ariane Weber:** Writing – review & editing, Writing – original draft, Methodology, Investigation, Formal analysis. **Rimantas Jankauskas:** Writing – review & editing, Resources. **Ronny Friedrich:** Writing – review & editing, Methodology, Formal analysis. **Kirsten I. Bos:** Writing – review & editing, Writing – original draft, Supervision, Funding acquisition, Resources, Project administration, Methodology, Conceptualization. **Denise Kühnert:** Writing – review & editing, Methodology.

Declaration of Competing Interest

The authors have no known competing interests to declare.

Acknowledgments

This work was funded by the Max Planck Society, the European Research Council (ERC) under the European Union's Horizon 2020 research and innovation programme Starting Grant agreement number 805268 CoDisEASe (to KIB), Social Sciences and Humanities Research Council of Canada Doctoral Scholarship 752–2016–0442 (to KG), Landesgraduiertenstipendium of the State of Thuringia and Friedrich-Schiller University Jena (to AW) and DAAD Doctoral Scholarship 57299294 (to KG). We thank Arthur Kocher, Aida Andrades Valtueña, Alexander Herbig and Thomas Lesley Sitter for technical assistance, and the laboratory technicians of the Max Planck Institute for Evolutionary Anthropology for assistance with data generation.

Author contributions

KIB and DK conceived of the investigation. JK and RJ performed osteological analyses and provided contextual information. KLG, AW, and RF performed experiments. KLG and KIB wrote the manuscript with contributions from all coauthors.

Appendix A. Supporting information

Supplementary data associated with this article can be found in the online version at doi:10.1016/j.ijpp.2025.11.002.

Data Availability

Raw DNA sequencing data from the above analyses can be found under the European Nucleotide Archive (ENA) accession number PRJEB80217. Molecular dating data (BEAST input configuration file, log and tree output files) can be found at https://github.com/tidelab/TreponemaDiffSampling_timeTree, or via https://doi.org/10.17617/3.DKYJVU, the data repository for the Max Planck Society.

References

Ambrose, S.H., 1990. Preparation and characterization of bone and tooth collagen for isotopic analysis. J. Archaeol. Sci. 17 (4), 431–451. https://doi.org/10.1016/0305-4403(90)90007-R.

Arora, N., Schuenemann, V.J., Jäger, G., Peltzer, A., Seitz, A., Herbig, A., Strouhal, M., Grillová, L., Sánchez-Busó, L., Kühnert, D., Bos, K.I., Davis, L.R., Mikalová, L., Bruisten, S., Komericki, P., French, P., Grant, P.R., Pando, M.A., Vaulet, L.G., Bagheri, H.C., 2016. Origin of modern syphilis and emergence of a pandemic Treponema pallidum cluster [Letter]. Nat. Microbiol. 2, 16245. https://doi.org/10.1038/nmicrobiol.2016.245.

Aufderheide, A.C., Rodriguez-Martin, C., 1998. The Cambridge Encyclopedia of Human Paleopathology. Cambridge University Press. ⟨http://tinyurl.sfx.mpg.de/v32j⟩.

Baker, B.J., Armelagos, G.J., Becker, M.J., Brothwell, D., Drusini, A., Geise, M.C., Kelley, M.A., Moritoto, I., Morris, A.G., Nurse, G.T., Powell, M.L., Rothschild, B.M., Saunders, S.R., 1988. The origin and antiquity of syphilis: paleopathological diagnosis and interpretation [and Comments and Reply. Curr. Anthropol. 29 (5), 703–737. https://doi.org/10.1086/203691.

Baker, B.J., Crane-Kramer, G., Dee, M.W., Gregoricka, L.A., Henneberg, M., Lee, C., Lukehart, S.A., Mabey, D.C., Roberts, C.A., Stodder, A.L., 2020. Advancing the understanding of treponemal disease in the past and present. Am. J. Phys. Anthropol. 171 (S70), 5–41.

Barquera, R., Lamnidis, T.C., Lankapalli, A.K., Kocher, A., Hernández-Zaragoza, D.I., Nelson, E.A., Zamora-Herrera, A.C., Ramallo, P., Bernal-Felipe, N., Immel, A., Bos, K., Acuña-Alonzo, V., Barbieri, C., Roberts, P., Herbig, A., Kühnert, D., Márquez-Morfín, L., Krause, J., 2020. Origin and health status of first-generation Africans from early colonial Mexico. e2011 Curr. Biol. 30 (11), 2078–2091. https://doi.org/10.1016/j.cub.2020.04.002.

Barquera, R., Sitter, T.L., Kirkpatrick, C.L., Ramirez, D.A., Kocher, A., Spyrou, M.A., Couoh, L.R., Talavera-González, J.A., Castro, M., von Hunnius, T., Guevara, E.K., Hamilton, W.D., Roberts, P., Scott, E., Fabra, M., Da Peña, G.V., Pacheco, A., Rodriguez, M., Aspillaga, E., Bos, K.I., 2024. Ancient genomes reveal a deep history

of treponemal disease in the Americas. Nature. https://doi.org/10.1038/s41586-024-08515-5.
Bos, K.I., Kühnert, D., Herbig, A., Esquivel-Gomez, L.R., Andrades Valtueña, A., Barquera, R., Giffin, K., Kumar Lankapalli, A., Nelson, E.A., Sabin, S., Spyrou, M.A., Krause, J., 2019. Paleomicrobiology: diagnosis and evolution of ancient pathogens. Annu. Rev. Microbiol. 73 (1), 639–666. https://doi.org/10.1146/annurev-micro-090817-062436.
Bos, K.I., Schuenemann, V.J., Golding, G.B., Burbano, H.A., Waglechner, N., Coombes, B. K., McPhee, J.B., DeWitte, S.N., Meyer, M., Schmedes, S., Wood, J., Earn, D.J.D., Herring, D.A., Bauer, P., Poinar, H.N., Krause, J., 2011. A draft genome of Yersinia pestis from victims of the Black Death. Nature 478, 506. https://doi.org/10.1038/nature10549.
Bouwman, A.S., Brown, T.A., 2005. The limits of biomolecular palaeopathology: ancient DNA cannot be used to study venereal syphilis. J. Archaeol. Sci. 32 (5), 703–713. https://doi.org/10.1016/j.jas.2004.11.014.
Briggs, A.W., Stenzel, U., Meyer, M., Krause, J., Kircher, M., Pääbo, S., 2009. Removal of deaminated cytosines and detection of in vivo methylation in ancient DNA. -e87 Nucleic Acids Res. 38 (6), e87. https://doi.org/10.1093/nar/gkp1163.
Brindzaitė, R., Motuzaitė Matuzevičiūtė, G., Jonaitis, R., Kaplūnaitė, I., Rudinska, A., Jakaitienė, A., Jankauskas, R., 2025. Dietary tendencies between social and religious groups in vilnius during the 13th–18th centuries (n/a(n/a)). Int. J. Osteoarchaeol.. https://doi.org/10.1002/oa.70028.
Brock, F., Higham, T., Ramsey, C.B., 2010. Pre-screening techniques for identification of samples suitable for radiocarbon dating of poorly preserved bones. J. Archaeol. Sci. 37 (4), 855–865. https://doi.org/10.1016/j.jas.2009.11.015.
Bronk Ramsey, C., 2009. Bayesian analysis of radiocarbon dates. Radiocarbon 51 (1), 337–360. https://doi.org/10.1017/S0033822200033865.
Bronk Ramsey, C., 2017. Methods for summarizing radiocarbon datasets. Radiocarbon 59 (6), 1809–1833. https://doi.org/10.1017/RDC.2017.108.
Brown, T.A., Nelson, D.E., Vogel, J.S., Southon, J.R., 1988. Improved collagen extraction by modified Longin Method. Radiocarbon 30 (2), 171–177. https://doi.org/10.1017/S0033822200044118.
Čejková, D., Zobaníková, M., Chen, L., Pospíšilová, P., Strouhal, M., Qin, X., Mikalová, L., Norris, S.J., Muzny, D.M., Gibbs, R.A., Fulton, L.L., Sodergren, E., Weinstock, G.M., Šmajs, D., 2012. Whole genome sequences of three treponema pallidum ssp. pertenue strains: yaws and syphilis treponemes differ in less than 0.2% of the genome sequence. PLOS Negl. Trop. Dis. 6 (1), e1471. https://doi.org/10.1371/journal.pntd.0001471.
Cockburn, T.A., 1961. The origin of the treponematoses. Bull. World Health Organ. 24 (2), 221–228. ⟨https://www.ncbi.nlm.nih.gov/pubmed/13694226⟩.
Cole, G., Waldron, T., Edwards, C., 2014. Letter to the editor: apple down 152 putative syphilis: pre-Colombian date confirmed. Am. J. Phys. Anthropol. 156. https://doi.org/10.1002/ajpa.22672.
Cole, G., Waldron, T., 2011. Apple down 152: a putative case of syphilis from sixth century AD Anglo-Saxon England. Am. J. Phys. Anthropol. 144 (1), 72–79. https://doi.org/10.1002/ajpa.21371.
DeWitte, S.N., Stojanowski, C.M., 2015. The osteological paradox 20 years later: past perspectives, future directions. J. Archaeol. Res. 23 (4), 397–450. https://doi.org/10.1007/s10814-015-9084-1.
Douglas, J., Zhang, R., Bouckaert, R., 2021. Adaptive dating and fast proposals: revisiting the phylogenetic relaxed clock model. PLOS Comput. Biol. 17 (2), e1008322. https://doi.org/10.1371/journal.pcbi.1008322.
Dutour, O. e, 1994. L'origine de la syphilis en Europe: avant ou après 1493?: actes du colloque international de Toulon, 25-28 novembre 1993. Editions Errance.
Erdal, Y.S., 2006. A pre-Columbian case of congenital syphilis from Anatolia (Nicaea, 13th century AD). Int. J. Osteoarchaeol. 16 (1), 16–33. https://doi.org/10.1002/oa.802.
Ewels, P.A., Peltzer, A., Fillinger, S., Patel, H., Alneberg, J., Wilm, A., Garcia, M.U., Di Tommaso, P., Nahnsen, S., 2020. The nf-core framework for community-curated bioinformatics pipelines. Nat. Biotechnol. 38 (3), 276–278. https://doi.org/10.1038/s41587-020-0439-x.
Fellows Yates, J.A., Lamnidis, T.C., Borry, M., Andrades Valtueña, A., Fagernäs, Z., Clayton, S., Garcia, M.U., Neukamm, J., Peltzer, A., 2021. Reproducible, portable, and efficient ancient genome reconstruction with nf-core/eager. PeerJ 9, e10947. https://doi.org/10.7717/peerj.10947.
Giffin, K., Lankapalli, A.K., Sabin, S., Spyrou, M.A., Posth, C., Kozakaitė, J., Friedrich, R., Miliauskienė, Ž., Jankauskas, R., Herbig, A., Bos, K.I., 2020. A treponemal genome from an historic plague victim supports a recent emergence of yaws and its presence in 15th century Europe. Sci. Rep. 10 (1), 9499. https://doi.org/10.1038/s41598-020-66012-x.
Gillespie, J.H., 1994. The Causes of Molecular Evolution. Oxford University Press.
Hackett, C.J., 1963. On the origin of the human treponematoses (Pinta, Yaws, Endemic Syphilis and Venereal Syphilis). Bull. World Health Organ. 29 (1), 7–41. ⟨https://www.ncbi.nlm.nih.gov/pubmed/14043755⟩.
Hackett, C.J., 1975. An introduction to diagnostic criteria of syphilis, treponarid and yaws (treponematoses) in dry bones, and some implications. Virchows Arch. A 368 (3), 229–241. https://doi.org/10.1007/BF00432525.
Hackett, C., 1976. Diagnostic Criteria of Syphilis, Yaws and Treponarid (Treponematoses) and of Some Other Diseases in Dry Bones: for Use in Osteoarchaeology. Springer Science and Business Media.
Harper, K.N., Zuckerman, M.K., Harper, M.L., Kingston, J.D., Armelagos, G.J., 2011. The origin and antiquity of syphilis revisited: an appraisal of old world pre-Columbian evidence for treponemal infection [https://doi.org/10.1002/ajpa.21613]. Am. J. Phys. Anthropol. 146 (S53), 99–133. https://doi.org/10.1002/ajpa.21613.
Hedges, R.E.M., Law, I.A., 1989. The radiocarbon dating of bone. Appl. Geochem. 4 (3), 249–253. https://doi.org/10.1016/0883-2927(89)90025-5.
Herbig, A., Maixner, F., Bos, K.I., Zink, A., Krause, J., Huson, D.H., 2016. MALT: fast alignment and analysis of metagenomic DNA sequence data applied to the Tyrolean Iceman. bioRxiv 050559. https://doi.org/10.1101/050559.
Hider, J., Duggan, A.T., Klunk, J., Eaton, K., Long, G.S., Karpinski, E., Giuffra, V., Ventura, L., Fornaciari, A., Fornaciari, G., Golding, G.B., Prowse, T.L., Poinar, H.N., 2022. Examining pathogen DNA recovery across the remains of a 14th century Italian friar (Blessed Sante) infected with Brucella melitensis. Int. J. Paleopathol. 39, 20–34. https://doi.org/10.1016/j.ijpp.2022.08.002.
Hillson, S., Grigson, C., Bond, S., 1998. Dental defects of congenital syphilis. Am. J. Phys. Anthr. 107 (1), 25–40. https://doi.org/10.1002/(sici)1096-8644(199809)107:1<25::Aid-ajpa3>3.0.Co;2-c.
Hübler, R., Key, F.M., Warinner, C., Bos, K.I., Krause, J., Herbig, A., 2019. HOPS: automated detection and authentication of pathogen DNA in archaeological remains. Genome Biol. 20 (1), 280. https://doi.org/10.1186/s13059-019-1903-0.
Hudson, E.H., 1946. Treponematosis. Oxford Medicine. Oxford University Press, pp. 9–122.
Hudson, E.H., 1963. Treponematosis and anthropology. Ann. Intern Med. 58, 1037–1048. https://doi.org/10.7326/0003-4819-58-6-1037.
Hudson, E.H., 1964. Treponematosis and African slavery. Br. J. Vener. Dis. 40 (1), 43–52. https://doi.org/10.1136/sti.40.1.43.
von Hunnius, T.E., Yang, D., Eng, B., Waye, J.S., Saunders, S.R., 2007. Digging deeper into the limits of ancient DNA research on syphilis. J. Archaeol. Sci. 34 (12), 2091–2100. https://doi.org/10.1016/j.jas.2007.02.007.
Hutchinson, J., 1858. Report on the effects of infantile syphilis in marring the development of the teeth. Trans. Pathol. Soc. Lond. 9, 449–455.
Joseph, S.K., Lindo, J., 2023. The evolutionary history of infectious disease in the ancient Americas and the pathogenic consequences of European contact. Am. J. Biol. Anthropol. 182 (4), 532–541. https://doi.org/10.1002/ajpa.24595.
van Klinken, G.J., 1999. Bone collagen quality indicators for palaeodietary and radiocarbon measurements. J. Archaeol. Sci. 26 (6), 687–695. https://doi.org/10.1006/jasc.1998.0385.
Kolman, C.J., Centurion-Lara, A., Lukehart, S.A., Owsley, D.W., Tuross, N., 1999. Identification of treponema pallidum subspecies pallidum in a 200-year-old skeletal specimen. J. Infect. Dis. 180 (6), 2060–2063. https://doi.org/10.1086/315151.
Kozlov, A.M., Darriba, D., Flouri, T., Morel, B., Stamatakis, A., 2019. RAxML-NG: a fast, scalable and user-friendly tool for maximum likelihood phylogenetic inference. Bioinformatics 35 (21), 4453–4455. https://doi.org/10.1093/bioinformatics/btz305.
Kromer, B., Lindauer, S., Synal, H.-A., Wacker, L., 2013. MAMS – A new AMS facility at the Curt-Engelhorn-centre for achaeometry, Mannheim, Germany. Nucl. Instrum. Methods Phys. Res. Sect. B Beam Interact. Mater. At. 294, 11–13. https://doi.org/10.1016/j.nimb.2012.01.015.
Livingstone, F.B., 1991. On the origin of syphilis: an alternative hypothesis. Curr. Anthropol. 32 (5), 587–590. https://doi.org/10.1086/204004.
Llanos-Lizcano, A., Hämmerle, M., Sperduti, A., Sawyer, S., Zagorc, B., Özdoğan, K.T., Guellil, M., Cheronet, O., Kuhlwilm, M., Pinhasi, R., Gelabert, P., 2025. Intra-individual variability in ancient plasmodium DNA recovery highlights need for enhanced sampling. Sci. Rep. 15 (1), 757. https://doi.org/10.1038/s41598-024-85038-z.
Loh, E., Salk, J.J., Loeb, L.A., 2010. Optimization of DNA polymerase mutation rates during bacterial evolution. Proc. Natl. Acad. Sci. USA 107 (3), 1154–1159. https://doi.org/10.1073/pnas.0912451107.
Majander, K., Pfrengle, S., Kocher, A., Neukamm, J., du Plessis, L., Pla-Díaz, M., Arora, N., Akgül, G., Salo, K., Schats, R., Inskip, S., Oinonen, M., Valk, H., Malve, M., Kriiska, A., Onkamo, P., González-Candelas, F., Kühnert, D., Krause, J., Schuenemann, V.J., 2020. Ancient bacterial genomes reveal a high diversity of treponema pallidum strains in early modern Europe. e3710 Curr. Biol. 30 (19), 3788–3803. https://doi.org/10.1016/j.cub.2020.07.058.
Majander, K., Pla-Díaz, M., du Plessis, L., Arora, N., Filippini, J., Pezo-Lanfranco, L., Eggers, S., González-Candelas, F., Schuenemann, V.J., 2024. Redefining the treponemal history through pre-Columbian genomes from Brazil. Nature. https://doi.org/10.1038/s41586-023-06965-x.
Meyer, M., Kircher, M., 2010. Illumina sequencing library preparation for highly multiplexed target capture and sequencing. Cold Spring Harb. Protoc. 2010 (6) pdb.prot5448.
Mitchell, P.D., 2003. Pre-Columbian treponemal disease from 14th century AD Safed, Israel, and implications for the medieval eastern Mediterranean. Am. J. Phys. Anthropol. 121 (2), 117–124. https://doi.org/10.1002/ajpa.10205.
Moon, H., 1877. On irregular and defective tooth development. Trans. Odontol. Soc. Gt. Br. 9.
Ortner, D.J., 2003. Infectious diseases: treponematosis and other bacterial infectious diseases. In: Ortner, D.J. (Ed.), Identification of Pathological Conditions in Human Skeletal Remains (Second Edition). Academic Press, pp. 273–323. https://doi.org/10.1016/B978-012528628-2/50048-X.
Paradis, E., Schliep, K., 2019. ape 5.0: an environment for modern phylogenetics and evolutionary analyses in R. Bioinformatics 35 (3), 526–528. https://doi.org/10.1093/bioinformatics/bty633.
Parker, C.E., Hiss, A.N., Spyrou, M.A., Neumann, G.U., Slavin, P., Nelson, E.A., Nagel, S., Dalidowski, X., Friederich, S., Krause, J., Herbig, A., Haak, W., Bos, K.I., 2023. 14th century Yersinia pestis genomes support emergence of pestis secunda within Europe. PLOS Pathog. 19 (7), e1011404. https://doi.org/10.1371/journal.ppat.1011404.
Parker, C., Rohrlach, A.B., Friederich, S., Nagel, S., Meyer, M., Krause, J., Bos, K.I., Haak, W., 2020. A systematic investigation of human DNA preservation in medieval skeletons. Sci. Rep. 10 (1), 18225. https://doi.org/10.1038/s41598-020-75163-w.

Peltzer, A., Jäger, G., Herbig, A., Seitz, A., Kniep, C., Krause, J., Nieselt, K., 2016. EAGER: efficient ancient genome reconstruction. Genome Biol. 17 (1), 60. https://doi.org/10.1186/s13059-016-0918-z.

Pětrošová, H., Zobaníková, M., Čejková, D., Mikalová, L., Pospíšilová, P., Strouhal, M., Chen, L., Qin, X., Muzny, D.M., Weinstock, G.M., Šmajs, D., 2012. Whole genome sequence of treponema pallidum ssp. pallidum, Strain Mexico A, suggests recombination between yaws and syphilis strains. PLOS Negl. Trop. Dis. 6 (9), e1832. https://doi.org/10.1371/journal.pntd.0001832.

Pinhasi, R., Fernandes, D., Sirak, K., Novak, M., Connell, S., Alpaslan-Roodenberg, S., Gerritsen, F., Moiseyev, V., Gromov, A., Raczky, P., Anders, A., Pietrusewsky, M., Rollefson, G., Jovanovic, M., Trinhhoang, H., Bar-Oz, G., Oxenham, M., Matsumura, H., Hofreiter, M., 2015. Optimal ancient DNA yields from the inner ear part of the Human Petrous bone. PLOS One 10 (6), e0129102. https://doi.org/10.1371/journal.pone.0129102.

Powell, M.L., Cook, D.C., 2005. The Myth of Syphilis: the Natural History of Treponematosis in North America. University Press of Florida.

Quétel, C., 1990. History of Syphilis. Johns Hopkins University Press. ⟨https://books.google.de/books?id=ZqLuAAAAMAAJ⟩.

Rao, V.V., Vasulu, T.S., Babu, A.D.W.R., 1996. Possible paleopathological evidence of treponematosis from a megalithic site at Agripalle, India. Am. J. Phys. Anthropol. 100 (1), 49–55. https://doi.org/10.1002/(SICI)1096-8644(199605)100:1<49::AID-AJPA5>3.0.CO;2-8.

Reimer, P.J., Austin, W.E.N., Bard, E., Bayliss, A., Blackwell, P.G., Bronk Ramsey, C., Butzin, M., Cheng, H., Edwards, R.L., Friedrich, M., Grootes, P.M., Guilderson, T.P., Hajdas, I., Heaton, T.J., Hogg, A.G., Hughen, K.A., Kromer, B., Manning, S.W., Muscheler, R., Talamo, S., 2020. The IntCal20 Northern Hemisphere Radiocarbon Age Calibration Curve (0–55 cal kBP). Radiocarbon 62 (4), 725–757. https://doi.org/10.1017/RDC.2020.41.

Reimer, P.J., Bard, E., Bayliss, A., Beck, J.W., Blackwell, P.G., Ramsey, C.B., Buck, C.E., Cheng, H., Edwards, R.L., Friedrich, M., Grootes, P.M., Guilderson, T.P., Haflidason, H., Hajdas, I., Hatté, C., Heaton, T.J., Hoffmann, D.L., Hogg, A.G., Hughen, K.A., van der Plicht, J., 2013. IntCal13 and marine13 radiocarbon age calibration curves 0–50,000 Years cal BP. Radiocarbon 55 (4), 1869–1887. https://doi.org/10.2458/azu_js_rc.55.16947.

Rohland, N., Harney, E., Mallick, S., Nordenfelt, S., Reich, D., 2015. Partial uracil–DNA–glycosylase treatment for screening of ancient DNA. Philos. Trans. R. Soc. B Biol. Sci. 370 (1660), 20130624. https://doi.org/10.1098/rstb.2013.0624.

Schuenemann, V.J., Kumar Lankapalli, A., Barquera, R., Nelson, E.A., Iraíz Hernández, D., Acuña Alonzo, V., Bos, K.I., Márquez Morfín, L., Herbig, A., Krause, J., 2018. Historic Treponema pallidum genomes from Colonial Mexico retrieved from archaeological remains. PLOS Negl. Trop. Dis. 12 (6), e0006447. https://doi.org/10.1371/journal.pntd.0006447.

Shennan, S., 1988. Quantifying Archaeology. Edinburgh University Press.

Spyrou, M.A., Bos, K.I., Herbig, A., Krause, J., 2019. Ancient pathogen genomics as an emerging tool for infectious disease research. Nat. Rev. Genet. 20 (6), 323–340. https://doi.org/10.1038/s41576-019-0119-1.

Spyrou, M.A., Keller, M., Tukhbatova, R.I., Scheib, C.L., Nelson, E.A., Andrades Valtueña, A., Neumann, G.U., Walker, D., Alterauge, A., Carty, N., Cessford, C., Fetz, H., Gourvennec, M., Hartle, R., Henderson, M., von Heyking, K., Inskip, S.A., Kacki, S., Key, F.M., Krause, J., 2019. Phylogeography of the second plague pandemic revealed through analysis of historical Yersinia pestis genomes. Nat. Commun. 10 (1), 4470. https://doi.org/10.1038/s41467-019-12154-0.

Spyrou, Maria A., Tukhbatova, Rezeda I., Feldman, M., Drath, J., Kacki, S., Beltrán de Heredia, J., Arnold, S., Sitdikov, Airat G., Castex, D., Wahl, J., Gazimzyanov, Ilgizar R., Nurgaliev, Danis K., Herbig, A., Bos, Kirsten I., Krause, J., 2016. Historical Y. pestis genomes reveal the European Black Death as the source of ancient and modern plague pandemics. Cell Host Microbe 19 (6), 874–881. https://doi.org/10.1016/j.chom.2016.05.012.

Steinbock, R.T., 1976. Paleopathological Diagnosis and Interpretation: Bone Diseases in Ancient Human Populations. Thomas. ⟨https://cir.nii.ac.jp/crid/1130000796598379008⟩.

Strouhal, M., Mikalová, L., Havlíčková, P., Tenti, P., Čejková, D., Rychlík, I., Bruisten, S., Šmajs, D., 2017. Complete genome sequences of two strains of Treponema pallidum subsp. pertenue from Ghana, Africa: identical genome sequences in samples isolated more than 7 years apart. PLOS Negl. Trop. Dis. 11 (9), e0005894. https://doi.org/10.1371/journal.pntd.0005894.

Villanueva, R.A.M., Chen, Z.J., 2019. ggplot2: elegant graphics for data analysis (2nd ed.). Meas. Interdiscip. Res. Perspect. 17 (3), 160–167. https://doi.org/10.1080/15366367.2019.1565254.

Wang, C., Cheng, Y., Liu, B., Wang, Y., Gong, W., Qian, Y., Guan, Z., Lu, H., Gu, X., Shi, M., Zhou, P., 2018. Sensitive detection of Treponema pallidum DNA from the whole blood of patients with syphilis by the nested PCR assay. Emerg. Microbes Infect. 7 (1), 1–7. https://doi.org/10.1038/s41426-018-0085-2.

Wang, C., Hu, Z., Zheng, X., Ye, M., Liao, C., Shang, M., Gong, W., Guan, Z., Lu, H., Gu, X., Shi, M., Zhou, P., 2021. A new specimen for syphilis diagnosis: evidence by high loads of treponema pallidum DNA in saliva. Clin. Infect. Dis. 73 (9), e3250–e3258. https://doi.org/10.1093/cid/ciaa1613.

Wang, C., Zheng, X., Guan, Z., Zou, D., Gu, X., Lu, H., Shi, M., Zhou, P., 2022. Quantified detection of treponema pallidum DNA by PCR assays in urine and plasma of syphilis patients. Microbiol Spectr. 10 (2), e0177221. https://doi.org/10.1128/spectrum.01772-21.

Ward, G.K., Wilson, S.R., 1978. Procedures for comparing and combining radiocarbon age determinations: a critique. Archaeometry 20 (1), 19–31. https://doi.org/10.1111/j.1475-4754.1978.tb00208.x.

Woolfit, M., 2009. Effective population size and the rate and pattern of nucleotide substitutions. Biol. Lett. 5 (3), 417–420. https://doi.org/10.1098/rsbl.2009.0155.

Žukovskis, R. 2007a. Aguonų g. 10, Vilniuje 2006 metais vykdytų archeologinių tyrimų ataskaita.

Žukovskis, R. 2007b. Aguonų g. 10, Vilniuje 2007 metų archeologinių tyrinėjimų ataskaita.